International Biodeterioration & Biodegradation 100 (2015) 124–132

Contents lists available at ScienceDirect

International Biodeterioration & Biodegradation

journal homepage: www.elsevier.com/locate/ibiod

Histological and ultrastructural alterations in the *Ailanthus excelsa* wood cell walls by *Bjerkandera adusta* (Willd.) P. Karst

S. Pramod [a], Rina D. Koyani [a], Isha Bhatt [a], Ajit M. Vasava [a], K.S. Rao [b], Kishore S. Rajput [a, *]

[a] Department of Botany, Faculty of Science, The Maharaja Sayajirao University of Baroda, Vadodara 390002, India
[b] Department of Biosciences, Sardar Patel University, VallabhVidyanagar 388120, India

ARTICLE INFO

Article history:
Received 30 April 2014
Received in revised form
13 February 2015
Accepted 14 February 2015
Available online 10 March 2015

Keywords:
Delignification
Simultaneous rot
Tree of heaven
White rot
Wood decay
Xylophagous fungus

ABSTRACT

Ailanthus excelsa Roxb. requires less care than other species and thrives in arid and semi-arid regions. Therefore, it becomes an important choice for forestry programs. Young branches of these trees are frequently invaded by the fungus *Bjerkandera adusta* (Willd.) P. Karst. The main aims of this study were to characterize the wood decay pattern and evaluate the extent of damage caused by the fungus. Infected samples were studied using light microscopy, confocal laser scanning microscopy, transmission electron microscopy, and scanning electron microscopy. Wood of the dead branches became pale white and very soft. In vitro decayed wood showed extensive weight loss of wood blocks (68.6%) at the end of three months. In the xylem, fibres were the most severely affected cell types, whereas wall structure of the axial parenchyma remained virtually unaltered. Unlike axial parenchyma, walls of the ray cells formed several boreholes and finally collapsed in the advanced stage of decay. By contrast, the middle lamella of all the xylem elements remained intact even at the end of three months. In the early stages of infection, vessels appeared to be resistant to the fungal action but they also became eroded at the advanced stage. The degradation pattern showed anatomical characteristics of both the white-rot and soft-rot type of decay. Thinning of walls from the lumen side and appearance of U-notches resembles white-rot decay, while tunnels through the S_2 layer of the fibre wall added the characteristics of the soft-rot decay pattern. Extensive weight loss of wood blocks following infection suggests *B. adusta* is an aggressive wood-degrading fungus.

Introduction

Ailanthus excelsa Roxb. (Simaroubiaceae) is a fast-growing multipurpose species cultivated in forestry programs in arid and semi-arid regions of India, including Gujarat state. It is extensively used as an avenue tree, in shelterbelts, in afforestation and reforestation programs, for silkworm culture, in biomass for fuel wood, and as a fodder source, and its bark also bears medicinal value (Elzaki and Khider, 2013). Wood of *A. excelsa* is used as a raw material for matchwood and plywood industries in India. In fully grown trees, dead branches are a frequent occurrence; these usually fall down during first showers of monsoon and due to high wind velocity. Such branches are light in weight, pale white, with very soft wood that can easily be crushed into powder with bare hands.

Bjerkandera adusta (Willd.) P. Karst is an aggressive pathogenic fungi and said to be dangerous to urban trees (Del Rio et al., 2002; Robles et al., 2011). The wood decay pattern of *B. adusta* has been studied previously and reported to cause white rot (Blanchette, 1984; Worall et al., 1997; Anagnost, 1998; Robles et al., 2014). On the basis of cell wall component removal, the modes of wood decay by xylophagous fungi are classified into white rot, soft rot, and brown rot (Blanchette, 1984; Worall et al., 1997; Anagnost, 1998). In white rot, cellulose, hemicelluloses, and lignin are degraded simultaneously or preferentially; thus the wood becomes soft, spongy, and white to pale white in color. The white-rot pattern is further classified as either simultaneous or selective rot. In the former type, all the cell wall components are removed at a more or less similar rate, while in the latter lignin may be removed preferentially from the cell walls (Robles et al., 2014). In brown rot, fungi remove cellulose and hemicelluloses, leaving behind oxidized lignin, which gives a brown color to the wood. In soft rot, cellulose, hemicellulose, and lignin are removed typically by tunneling

* Corresponding author. Tel.: +91 265 2791891; fax: +91 265 2792277.
E-mail address: ks.rajput15@yahoo.com (K.S. Rajput).

http://dx.doi.org/10.1016/j.ibiod.2015.02.026
0964-8305/

activity or formation of erosion troughs in the S_2 layer of secondary walls (Schwarze, 2007).

There is no unanimous opinion regarding the pattern of delignification of wood by *B. adusta*. According to Anagnost (1998) and Robles et al. (2014), it is a simultaneous delignifier, while Blanchette (1984) reported that it causes selective delignification. In the present study, the fungus shares the characteristics of both simultaneous white rot and soft rot. Therefore, the main objectives of this study were to: (1) describe anatomical alterations induced in the woody cell walls of *A. excelsa* by *B. adusta* using light microscopy (LM), confocal laser scanning microscopy (CLSM), scanning electron microscopy (SEM), and transmission electron microscopy (TEM); and (2) evaluate the potential of *B. adusta* to produce lignin-degrading enzymes.

Materials and methods

Plant material

Wood samples from the fallen trees and branches of *A. excelsa* Roxb. growing on the campus and in the botanical garden of the M. S. University of Baroda, Gujarat, India, were collected. The sap wood of *A. excelsa* is characterized by a typical hard wood tissue composed of vessels, fibres, and axial and ray parenchyma cells. Immediately after collection some of the samples were fixed in formaldehyde-acetic acid-alcohol solution (Berlyn and Miksche, 1976) for light microscopic study and in 0.1% glutaraldehyde for semi-thin sections and EM studies. The rest of the unfixed samples were used to isolate the causal organism.

Isolation and identification of fungi

Wood disks of the fallen branches were collected and small pieces of the wood were inoculated on malt extract agar media (MEA) to isolate the causal organism. Molecular analysis of the ITS region of ribosomal RNA was used to identify the fungus, which was found to be *B. adusta* (Willd.) Karst. The sequences generated in this study were deposited in the NCBI-GenBank with the accession number KJ606691. The phylogenetic tree was constructed using MEGA 5 software and the evolutionary history was inferred by using the Maximum Likelihood method based on the Tamura-Nei model (Tamura and Nei, 1993).

In-vitro decay test

Wood discs harvested from the main trunk of freshly cut 12–15-yr-old healthy *A. excelsa* Roxb. trees were obtained from the Forest Department Research nursery wood depot at Mahesana (Gujarat state, India). These wood discs were cut into cubic pieces measuring 20 × 20 × 20 mm, oven-dried at 50 °C for 72 h, and then stored at room temperature. Prior to inoculation with *B. adusta*, 64 (16 control and 48 experimental) cubic blocks were immersed in sterile water for 24 h to provide the ideal moisture level to facilitate fungal action. The weight loss of the wood blocks after regular intervals of in-vitro decay testing was determined as per the methodology described by Sanghvi et al. (2013) and Koyani and Rajput (2014). Before rewetting, 12 wood blocks (three for every 30 days) were marked and weighed to determine the initial dry weight. The same blocks were employed after the experiment to obtain the final dry weight. Rewetted blocks were autoclaved at 120 °C for 30 min, and surface-sterilized as described above. Four blocks were kept in an autoclaved petri plates containing 2.5% malt extract agar (MEA) medium. Each block was inoculated with 15-day-old cultures of *B. adusta* and maintained at 27 °C and 70% relative humidity. Inoculated samples along with controls were harvested at monthly intervals for four months. The harvested samples were cleaned gently with a brush to remove the surface mycelia and fixed in FAA (Johansen, 1940) and 0.1% glutaraldehyde in sodium cacodylate buffer (pH 7.2). Marked blocks were dried at 70 °C for 48 h and weighed to obtain the final dry weight. Percentage weight loss for each block was calculated as described by Koyani and Rajput (2014).

Sample processing

Wood samples measuring approximately 2 × 5 mm were trimmed and fixed in a mixture of 0.1% glutaraldehyde and 4% paraformaldehyde in 50 mM sodium cacodylate buffer for 4 h at room temperature. After washing in buffer, samples were dehydrated in a graded series of ethanol (30–95%, 15 min each, pure ethanol × 3, each for 20 min) infiltrated with a mixture of LR white and ethanol (V/V) 1:3, 1:1,3:1 and pure resin (4 days in each solution). Embedding was done in fresh LR white (London Resin, hard grade) using gelatin capsules, and capped capsules were left in an oven at 60 °C for polymerization for 2 days.

Light microscopy

For bright field microscopy samples were processed through a tertiary butyl alcohol series (Johansen, 1940). Details of the sectioning and staining are described elsewhere (Koyani and Rajput, 2014). Semi-thin (1–2-μm) sections of samples embedded in LR white were taken with a glass knife using an ultramicrotome (RMC, Powertome X, USA) and stained with Toluidine blue O. Stained sections were observed and photographed using a Leica DM 2000 microscope with a Cannon DC 150 digital camera (Germany) attached.

Confocal laser scanning microscopy (CLSM)

Hand sections (approximately 40–80 μm thickness) taken from the wood blocks washed in water and 0.01 M phosphate buffer (pH 9.0) were mounted in Fluoroshield mounting medium (Sigma, Germany) on a glass slide. Slides were examined with a Zeiss CLSM using a Krypton/argon laser emitting at wavelength of 488 and 568 nm (Donaldson and Lausberg, 1998).

Scanning electron microscopy (SEM)

For SEM studies, glutaraldehyde-fixed samples were cut into 2–3 mm^2 cubes having a thickness of about 3 mm, dehydrated in graded series of acetone, acetone-amyl acetate, and dried at room temperature. After mounting on aluminum stubs they were coated with gold using a Quaram sputter-coating unit, (Model SC 7610, U.K.) and observed and photographed with a LEO 440i SEM at 10 kV.

Transmission electron microscopy (TEM)

Ultrathin sections of 60–80 nm thickness taken from LR-white-embedded samples were collected on nickel grids and stained with 0.1% $KMnO_4$ in citrate buffer for lignin (Donaldson, 1992). Observations were made using TEM (Philips Tecnai 20, The Netherlands) at an acceleration voltage 80 kV, and electron micrographs were obtained using a CCD camera (Mega View III, Olympus Soft Imaging Solutions, USA).

Results

In-vitro decay test

Naturally infected wood disks were pale white, very soft, and light in weight; therefore a greater weight loss would be expected

in inoculated wood blocks than in naturally infected ones. The wood blocks were completely ramified with mycelial growth within the first week of inoculation. Un-inoculated wood blocks (control) showed negligible weight loss, i.e., 0.73–1.68% from 30 to 120 days, whereas inoculated blocks showed a faster rate of weight loss than did control blocks until day 60; thereafter, the weight loss slowed down. After 30 days of inoculation about 24% weight loss was observed; this subsequently increased to about 45%, 59%, and 69% after 60, 90, and 120 days of incubation, respectively.

Light microscopy

Sections taken from the wood of naturally infected trees showed anatomical characteristics usually found in simultaneous white rot such as formation of erosion channels with round edges and widening of pit regions between rays and fibres (Fig. 1a). Severely degraded samples showed merging of erosion channels resulting in large void areas within the secondary wall of fibres (Fig. 1b). Tangential sections showed degradation of the wall across the angle of cellulose microfibrils in fibres, indicating a typical soft-rot type 1 decay pattern (Fig. 1c).

The examination of experimental samples revealed that the mycelial invasion in the wood blocks occurs mainly through the lumen and bordered pits on the lateral walls of vessels, while radial movement of mycelia takes place through the rays. During the initial stages of wood decay, ray cell and vessel walls were intact and deeply stained, indicating the resistance of these walls to degradation (Fig. 2a). In contrast, the fibres formed erosion troughs in the wall by extensive removal of secondary wall material due to simultaneous degradation of wall polymers (Fig. 2b). Erosion troughs were formed from the lumen toward middle lamellae and fungal hyphae were found within the degraded secondary wall region (Fig. 2b). Advanced thinning resulted in localized removal of cell wall and middle lamellae, forming erosion channels through which fungal mycelia migrated to adjacent cells (Fig. 2b). Apotracheal parenchyma showed fungal hyphae attached to the inner wall region that traversed into the adjacent ray cells through breaks in the wall, resulting in simultaneous decay (Fig. 2c). Although non-contact ray cells were less prone to wall degradation during initial stages, the contact rays exhibited wall degradation and fungal hyphae appear to be migrating from ray to paratracheal cells (Fig. 2c). The tangential longitudinal sections also revealed colonization of fungal hyphae within ray cells and erosion holes in the cell walls (Fig. 2d). In transverse view, erosion channels on the fibre wall appeared as U-shaped notches while the vessel wall showed several intermittent gaps, indicating degradation of the cell wall and pit erosion (Fig. 2e).

During the advanced stages of decay, extensive wall degradation of fibres, vessels, and ray cells was apparent, while the walls of the axial parenchyma remained relatively unaltered. The fibre walls showed two kinds of degradation pattern within the same wood block. In some of the fibres, degradation started from the S_1 region of the wall, leaving small gaps between compound middle lamellae and the major part of the secondary wall (Fig. 2f). In the second pattern, large boreholes were noticed in the S_2 layer and progressive decay of the S_2 wall region, forming a large gap between the compound middle lamellae and the S_3 layer (Fig. 2f). The tip of the erosion channels showed rounded edges resembling typical simultaneous degradation by white-rot fungi (Fig. 2e). The vessel wall revealed degradation of the S_2 wall layer, which appeared as small holes in between secondary wall layers (Fig. 2g). Migration of fungal hypha from vessel into associated parenchyma through eroded pit was observed frequently in all the samples investigated. By contrast, the parenchyma cells away from the vessel wall were found with intact walls (Fig. 2g). Among all the cell types of secondary xylem, fibres were more vulnerable than axial parenchyma, which is a cell type relatively resistant to fungal action.

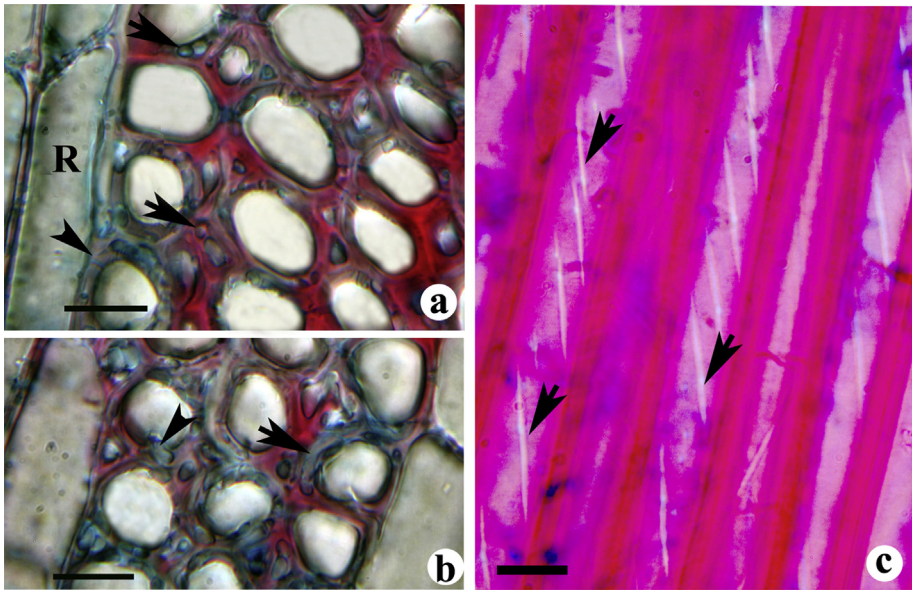

Fig. 1. (a–c). Transverse (a, b) and tangential longitudinal (c) sections of *A. excelsa* wood naturally infected by *B. adusta*.

a. Fibres showing erosion channels with rounded edges within the secondary wall (arrows). Arrow head indicates the widening of pit region in the wall between walls of ray (R) and fibre.
b. Large void areas formed in the secondary wall of fibres through merging of erosion channels (arrow). Arrow head indicates the erosion channels formed across the wall between the fibres.
c. Degradation of wall along the angle cellulose microfibrils in the fibre walls (arrows).
Scale bar = 20 μm.

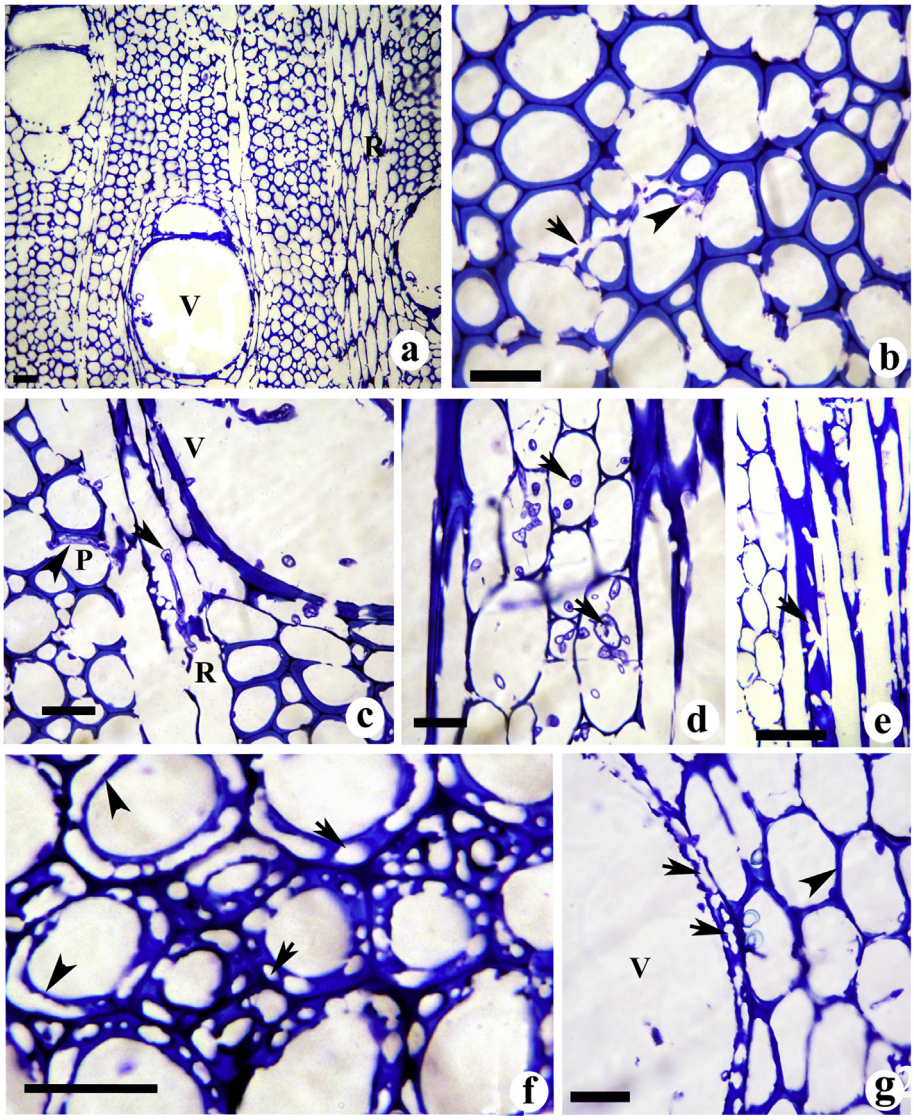

Fig. 2. (a–g). Transverse (a–c, f–g) and tangential longitudinal (d, e) sections from the wood of *A. excelsa* infected by *B. adusta*.

a. Fibres, vessels (V), and vessel-associated parenchyma and contact ray (R) showing cell wall degradation at the early stages of infection. Note the less damaged cell wall in non-contact rays.
b. Fibres showing degradation of cell corner regions (arrows) and breaking of cell walls following complete removal of secondary wall material. Arrowhead indicates the fungal hyphae in association with damaged cell walls.
c. Fungal hypha (arrow) with a tip projecting into the ray cell lumen (R). Arrowhead indicates the hypha continuous between ray and parenchyma. Note the hyphae attached to the inner wall of parenchyma cell and tip is crossing the adjacent cell through the broken wall area.
d. Ray cells showing fungal mycelia inside the lumen (arrows). Note the boreholes in the fibre wall.
e. Fibre showing erosion channels with U-notches in the secondary wall (arrow).
f. Erosion troughs in fiber secondary walls (arrows) and large holes formed after complete degradation of $S_1 + S_2$ layers. Arrowheads indicate the intact S3 layer at an advanced stage of fibre wall degradation.
g. Vessel (V) wall showing degradation of S_2 layer of secondary wall resulting in large gaps in middle layers wall (arrows). Arrowhead indicates the parenchyma cell wall with less damage.
Scale bar: a, f = 50 μm; b–e and g–i = 25 μm.

Confocal laser scanning microscopy (CLSM)

Examination with CLSM revealed the differences in the auto-fluorescence pattern during the delignification process in different cell types attacked by *Bjerkandera adusta*. The secondary wall regions of fibre showed non-fluorescent regions of boreholes while no alternation in lignin distribution was evident in ray cell walls (Fig. 3a). Fungal mycelia not only form vertical tunnels through the fibre walls but also develop horizontal tunnels of irregular shape and size in the S_2 layer (Fig. 3a). In some of the fibres the tunnels were observed in the S_2 layer but left the S_3 and S_1 layers intact, indicating the typical soft-rot pattern with "L" and "T" bending (Fig. 3a). Some of the tunnels showed narrow-diameter holes in the S_3 layer that became larger in the S_2 layer, indicating that mycelia entered from the lumen side by forming transverse borehole and bends in vertical or horizontal direction. The compound middle lamellae and cell corners of fibres produced a high intensity of fluorescence due to higher lignin concentration, which was unaltered, while the secondary wall underwent simultaneous degradation by removal of all components of the cell wall (Fig. 3b). The

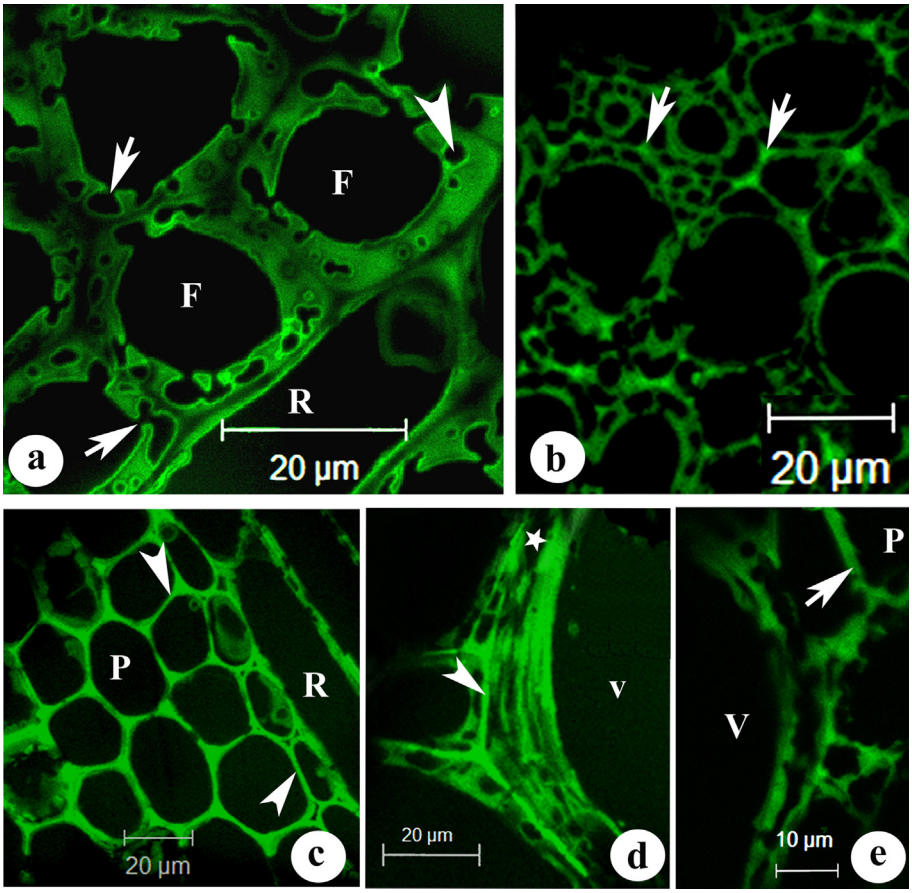

Fig. 3. (a–e). Confocal images of transverse sections from the wood of *A. excelsa* infected by *B. adusta*.

a. The erosion channels formed near the cell corner (arrowhead) and secondary wall (arrows) of fibres (F). Note the rays (R) showing relatively less damage to the lignified, thin secondary wall.
b. Fibres showing extensive damage in inner secondary wall regions during advanced stage of decay. Arrows indicate high fluorescence from intact middle lamellae regions.
c. The axial parenchyma (P) showing highly fluorescent, thin secondary wall without damage (arrowheads).
d. The vessel (V) wall showing absence of fluorescence from the degraded part of secondary wall. Arrowhead indicates the high fluorescence from the intact middle lamella region. Note the large pore (asterisk) formed following pit erosion and subsequent decay into secondary wall of vessel.
e. The non-fluorescent regions of S2 layer of vessel showing wall degradation during advanced stage. Arrow indicates relatively high fluorescence from the wall of parenchyma cell (P) away from the vessel.

advancement of wall degradation within the middle part of the secondary wall was evident from the presence of non-fluorescent regions between high-intensity fluorescence in the compound middle lamellae and S_3 wall layer (Fig. 3c). The axial parenchyma cells showed uniform fluorescence throughout the wall, indicating no alternation in wall chemistry (Fig. 3d). In the advanced stages of decay, vessel walls also became susceptible to ligninolytic activity of fungal enzymes. At this stage, the compound middle lamellae and inner part of the S_3 wall region showed more fluorescence intensity, while patches of non-fluorescent regions were apparent in S_1 and the outer region of S_2 wall layers (Fig. 3e). During the advanced stages of decay, a complete non-fluorescent region appeared in the S_2 layer of vessel; this spread into the compound middle lamellae and secondary wall of adjacent parenchyma cells, resulting in a gap in the wall between them (Fig. 3e).

Scanning electron microscopy

Analysis with SEM revealed the colonization of fungal mycelia within the vessel lumen. Contact rays showed erosion of pits and large boreholes on both radial and tangential walls that facilitate further invasion of fungal mycelia into adjacent axial elements (Fig. 4a). Sometimes, two or three or more boreholes fuse together and form large holes on the ray cell walls (Fig. 4a). It is evident from Fig. 4b and c that mycelia migrate via simple pits of the ray cells by eroding the pit membranes. As observed under light microscopy, SEM studies also revealed thinning of the fibre wall from the lumen side toward the middle lamellae by formation of erosion troughs (Fig. 4d). Fungal hypha passing through the boreholes in the fibre wall into adjacent cells was apparent during progression of the decay process (Fig. 4e). The speeding of degradation across the wall resulted in transversely elongated boreholes in fibres (Fig. 4f). The erosion of the lumen surface leads to even thinning of walls as opposed to channel formation (Fig. 4f).

Transmission electron microscopy

Ultrathin sections of degraded wood stained with $KMnO_4$ were analyzed with TEM, which revealed the structural alterations in the cell wall and the pattern of delignification during the wood decay process. Following the attachment of fungal hyphae to the cell wall, electron translucent regions were observed in the secondary wall region (Fig. 5a). The simultaneous degradation of wall polymers was evident from the large electron translucent regions in the S_2 layer of fibres (Fig. 5b). Transverse sections showed the penetration of mycelia through the erosion channels in the secondary wall,

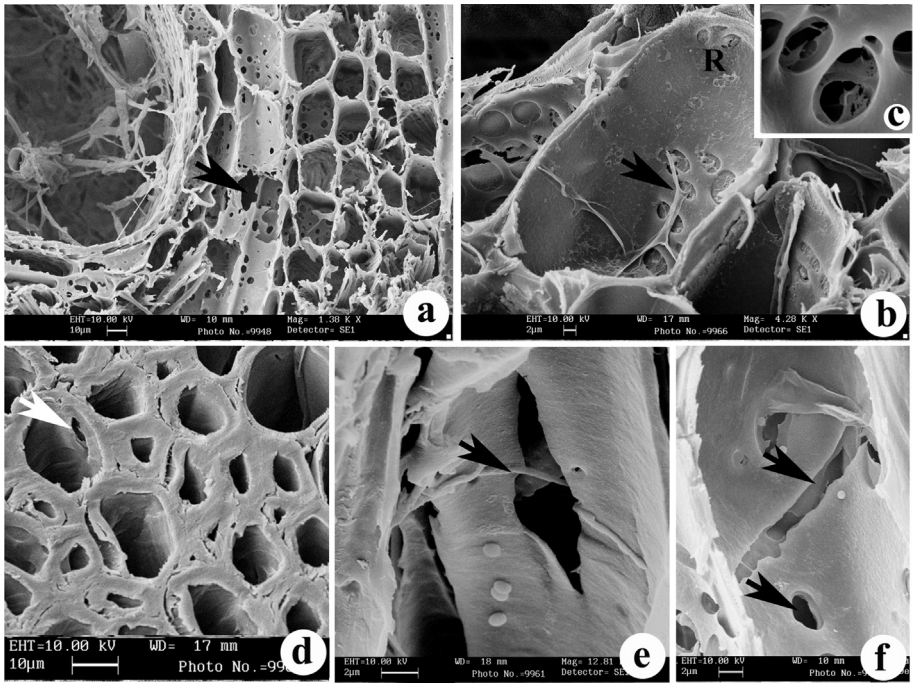

Fig. 4. (a–f). Scanning electron micrographs from the wood of *A. excelsa* infected by *B. adusta*.

a. Vessel showing the colonization of fungal mycelia in lumen. Arrow indicates the large holes formed in the rays.
b. Ray cell showing hyphal migration to adjacent cell through pits (arrow).
c. Erosion of pit membranes in simple pits of axial parenchyma.
d. Fibre showing the boreholes (arrow).
e. Fungal hyphae (arrow) passing through the large borehole in the fibre wall.
f. Fibre wall erosion from lumen side (arrows).

confirming progression of wall degradation across the cell wall (Fig. 5c). Hyphae were also observed passing through separated cells by degrading the compound middle lamellae region (Fig. 5d). Electron dense region of cell corners suggested relatively more lignin distribution in this particular area (Fig. 5e). The boreholes across S_2 and S_3 layers were apparent in the fibre wall, whereas the adjacent parenchyma had relatively thin secondary wall with intact wall layers (Fig. 5e). During the advanced stages of borehole expansion, the lignin-rich cell corners remained unaltered, indicating more decay resistance of the wall polymers due to its composition in this region (Fig. 5f). Simultaneous degradation of fibre walls left patches of secondary wall and relatively intact, electron dense middle lamella during the advanced stages of decay (Fig. 5g).

Discussion

The resistance of any wood species to microbial invasion and resultant degradation of wood depends upon its natural durability, genetic constitution, stored cell extractives, and composition of cell wall polymers (Sanghvi et al., 2013). Besides the inbuilt mechanism of host resistance to pathogen attack, the ability of the fungus to overcome the inhibition mechanism also plays an important role in the host–pathogen interaction. In the present study, naturally infected wood becomes pale white and very soft. An in-vitro decay test also supports the assertion that *B. adusta* is an extensive cell wall lignin degrader. Recently Robles et al. (2011, 2014) studied the pattern of wood decay caused by *B. adusta* in street trees in Buenos Aires, Argentina, and reported it to be caused by a very aggressive pathogenic fungus. In the present investigation, it was found that the rate of weight loss of wood blocks was higher than in the initial two months of inoculation; thereafter it became slow and about 69% of weight loss was observed after 120 days' incubation. Similar behavior has also been reported in the wood blocks of *Populus* and *Salix* wood inoculated with *Trametes trogii* (Anselmi and Nicolotti, 1990; Levin and Castro, 1998). In contrast, initial weight loss may be slow due to availability of several low-molecular-weight compounds available in the wood (Fengel and Wegener, 1989; Worall et al., 1997). Our result supports the hypothesis that the process of delignification and average weight loss depends upon the type of wood, ability of the fungus, and time (Adaskaveg et al., 1995).

The decay pattern of *Bjerkandera adusta* in the *Ailanthus* wood revealed typical simultaneous rot of cell wall polymers resulting in degradation of the entire cell wall. Previous reports on the decay pattern exhibited by this fungus are contradictory. In *Betula papyrifera*, it caused selective delignification resulting in dissolution of middle lamellae and defibration of cells (Blanchette, 1984). By contrast, our results are in agreement with Anagnost (1998), who reported that *B. adusta* caused simultaneous rot in *Betula alleghaniensis*, producing erosion channels within cell walls and pit fields. Similar results have also been reported by Robles et al. (2014) regarding degradation of London plane wood (*Platanus acerifolia*) by *B. adusta*. However, our results regarding ray cells differ from those of Robles et al. (2014). According to them, ray cells remained unaffected by mycelial action of *B. adusta*. Our observations revealed that at an advanced stage of decay, ray cells were severely affected and formed several boreholes. Sometimes two to three boreholes fused to form large cavities. This appears to be associated with the cell extractives stored in the parenchyma, which differ from species to species. Durability of the wood and its resistance to fungal attack is correlated with the nature and amount of extractives stored in wood parenchyma of soft wood and hard wood species (Bhat et al., 2005).

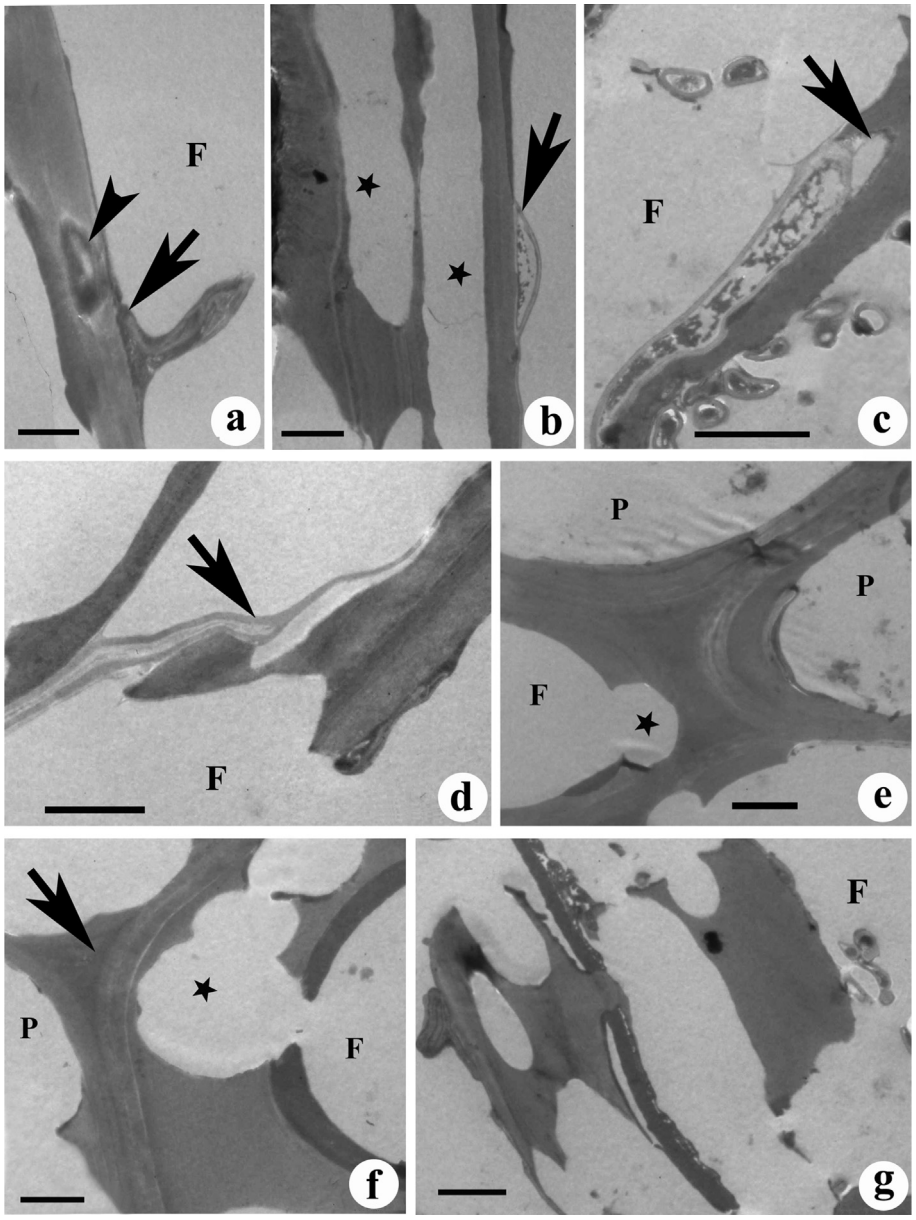

Fig. 5. (a–f). Transmission electron micrographs from the wood of *A. excelsa* infected by *B. adusta*.

a. Electron translucent regions in the secondary wall of fibre (F, arrowhead). Arrow indicates the fungal hypha along the inner wall.
b. Degradation of S2 layer of fibres (F) resting in large holes (asterisks). Arrow indicates the fungal mycelia.
c. Fungal hypha (arrow) penetrating across the wall of fibres (F).
d. The localized removal of cell wall and middle lamellae of fibres (F). Arrow indicates the hypha.
e. Borehole (asterisk) in the secondary wall of fibre (F). Note the intact wall of parenchyma cell (P) with relatively thin secondary wall.
f. Enlarged view of erosion trough in the fibre (F) secondary wall (asterisks). Note the electron-dense region of cell corner showing less degradation.
g. The remnants of cell wall of fibre (F) during advanced stages of decay. Note the electron-dense compound middle lamellae region.
Scale bar: a, d, f = 1 μm; b, c, e, and g = 2 μm.

The non-contact rays and axial parenchyma in *Ailanthus* showed resistance to degradation until the advanced stage of decay. Schwarze and Fink (1997) reported that the degradation resistance of xylem rays in London plane wood infected with *Inonotus hispidus* could be associated with the formation of polyphenol deposits in the lumina of cells. The defensive nature of polyphenolic compounds in living parenchyma and their relatively thin secondary wall (a lesser nutritional source in the form of cell wall polymers) may plausibly result in inhibition of fungal preference for these cell types. The contact ray and vessel associated parenchyma cells, on the other hand, showed degradation of cell walls. This could be associated with the channels necessary for axial and radial spreading of fungal mycelia from vessels to fibres and vice versa. Scanning electron microscopy also revealed the intercellular migration of fungal mycelia through erosion of membranes in simple pit. Pit erosion has been found to be a common feature of wood decay by white-rot fungi (Schwarze, 2007). Though cell wall chemistry of parenchymatous cells may be less affected during the decay process by *B. adusta*, their pit fields may form the easiest migration channels for movement toward preferred cell types such as fibres and vessels.

During the initial stages of decay, vessels showed resistance to degradation while the fibre wall was more prone to decay. In

general, vessels are highly resistant to attack by white-rot fungi. This decay resistance has been attributed to an increase in the concentration and monomeric composition of lignin in vessel walls. The vessels are generally characterized by a relatively higher amount of guaiacyl/syringyl lignin monomer ratio than that of other cell types (Blanchette et al., 1987). The guaiacyl lignin seems to be more difficult to degrade because of its more condensed structural configuration compared to the less complex nature of syringyl lignin units, which are predominantly found in the secondary wall of fibres (Blanchette et al., 1990). Confocal microscopy revealed a high-intensity autofluorescence from the decay-resistant region of compound middle lamellae and S_3 layer of fibres and vessel wall. The variation in intensity of autofluorescence from lignin is related to its concentration and monomeric composition (Micco and Aronne, 2007). Therefore, the greater vulnerability of fibre walls to fungal attack compared to the guaiacyl-lignin-rich vessel wall and compound middle lamellae region might be related to the variation in lignin concentration and its monomeric composition. Similar correlation has also been established by earlier workers (Iiyama and Pant, 1988; Luján et al., 2004; Koyani et al., 2010; Koyani and Rajput, 2014).

Transmission electron microscopy of $KMnO_4$-stained sections reveals electron translucent regions in the cell walls indicating the removal of lignin and suggests the strong ligninolytic activity of *B. adusta*. Ward et al. (2004) studied the enzyme profile of this species and reported various ligninolytic enzymes such as lignin peroxidase, manganese peroxidase, and versatile peroxidase. The presence of an electron-dense area in the cell corner of compound middle lamellae also supports the hypothesis that concentration of monomers of guaiacyl lignin may play a role in resistance to decay in this region. Generally, fungus moves along the length of the cell during the degradation process; however, TEM observation of transverse sections suggests that *B. adusta* also moves across the cell walls.

The degradation of the fibre wall in *Ailanthus* revealed three distinct patterns: (1) degradation of the S_1 layer and progression toward inner layers leading to thinning of walls; (2) formation of erosion channels in the S_2 layer and their extension, resulting in the layer's complete removal, often leaving compound middle lamellae intact; and (3) degradation from the lumen surface (S_3 layer) toward outer wall layers, leading to thinning of walls. Schmitt et al. (2014) observed degradation resistance of the S3 layer of fibres during early stages of decay while a complete loss of secondary wall and unaffected compound middle lamellae during the advanced stage was evident, suggesting high resistance of lignin-rich portions to soft-rot decay caused by *Spanchnonema platani* in plane trees. In the present study, boreholes and erosion troughs found in the cell walls appear to be typical of simultaneous white-rot-type decay. The important white-rot features during simultaneous decay include appearance of erosion troughs with rounded edges in transverse and U-notches in tangential sections, erosion of lumen surface resulting in wall thinning, and localized removal of cell walls and middle lamellae (Anagnost, 1998). Although *B. adusta* shows these features of white-rot decay, they also exhibit some features characteristics of soft rot. The boreholes in the S_2 layer, leaving the S_3 layer and compound middle lamellae unaltered, are typically found in the soft-rot of type of decay (Anagnost, 1998). Soft-rot decay caused by basidiomycetes is uncommon. Our results suggest *B. adusta* shares the characteristics of both soft and white rot during decay of *Ailanthus* wood. Similar features were also reported in ash wood during decay by *Inonotus hispidus* (Schwarze et al., 1995). The brown-rot fungi *Coniphora puteana* has been reported to cause a soft-rot decay pattern in sapelli wood under wet condions (Kleist and Schmitt, 2001). During the facultative mode of degradation, the restriction of gaseous exchange within the cell lumen due to high moisture content in the decay environment, as well as physical, micro-morphological, and chemical wood properties, influence the soft rot attack more than white rot attack (Schwarze et al., 1995) or brown-rot (Kleist and Schmitt, 2001) mode of wood decay. Our results are in agreement with these reports, and this study demonstrates the ability of facultative mode of decay by the xylophagous fungus *B. adusta* during degradation of *Ailathus* wood.

In conclusion, the present study demonstrates that *B. adusta* causes simultaneous rot in the wood of *A. excelsa*. However, the degradation pattern at an advanced stage of decay suggests that it shares the characteristics of both the soft- and white-rot type of decay. Among the different cell types, the secondary wall of fibres is more prone to decay from the initial stage while non-contact rays and axial parenchyma resists degradation until the advanced stage of decay. Confocal and TEM studies show the wall regions of high lignin distribution such as the vessel wall and compound middle lamellae are relatively resistant to degradation. The higher percentage of weight loss by *B. adusta* in *Ailanthus* wood suggests that this could be a potentially aggressive decay fungi with high ligninolytic activity. This study also highlights the need to monitor the spreading pattern and host nature of this fungus in urban parts of Baroda, India, where a large number of *Ailanthus* trees are grown under a forestry program.

Acknowledgements

Thanks are due to Council of Scientific and Industrial Research (CSIR) for financial support given to KSR and University Grants Commission (UGC), New Delhi for the award of Dr. D. S. Kothari Post-doctoral fellowship to PS. The authors are grateful to the anonymous reviewers, to Dr. Christine Gaylarde (editor), to the DBT-ILSPARE central instrumentation facility, and to Ms. Komal Raval for technical assistance.

References

Adaskaveg, J.E., Gilbertson, R.L., Dunlap, M.R., 1995. Effects of incubation time and temperature on in vitro selective delignification of silver leaf Oak by *Ganoderma colossum*. Appl. Environ. Microbiol. 6 (1), 138–144.
Anagnost, S.E., 1998. Light microscopy diagnosis of wood decay. Int. Assoc. Wood Anatom. J. 19, 141–167.
Anselmi, N., Nicolotti, G., 1990. Biological aspects and biodegradatory activities on poplar wood of *Trametes trogii* Berk. Mater. Org. 25, 71–80.
Bhat, K.M., Thulasidas, P.K., Maria, F.E.J., Jayaraman, K., 2005. Wood durability of home-garden teak against brown-rot and white-rot fungi. Trees 19, 654–660.
Blanchette, R.A., 1984. Screening of wood decay by white rot fungi for preferential lignin degradation. Appl. Environ. Microbiol. 48, 647–653.
Blanchette, R.A., Obst, J.R., Hedger, J.I., Weliky, K., 1987. Resistance of hard wood vessels to degradation by white rot basidiomycetes. Can. J. Bot. 66, 1841–1847.
Blanchette, R.A., Abad, A., Nilsson, T., Daniel, D., 1990. Biological degradation of wood. In: Rowel, R.M., Barbour, R.J. (Eds.), Archeological Wood: Properties, Chemistry and Preservation, Adavances in Chemistry Series, vol. 225. American Chemical Society, Washington DC, pp. 141–174.
Berlyn, G.P., Miksche, J.P., 1976. Botanical Microtechnique and Cytochemistry. The Iowa State University Press, Ames, Iowa.
Donaldson, L.A., 1992. Lignin distribution during late wood formation in *Pinus radiata* D. Don. Int. Assoc. Wood Anatom. J. 13 (4), 381–387.
Donaldson, L.A., Lausberg, M.J.F., 1998. Comparison of conventional transmitted light and confocal microscopy for measuring wood cell dimensions by image analysis. Int. Assoc. Wood Anatom. J. 19, 321–336.
Del Rio, J.C., Speranza, M., Gutierrez, A., Martinez, M.J., Martinez, A.T., 2002. Lignin attack during eucalypt wood decay by selected basidiomycetes: a Py-GC/MS study. J. Anal. Appl. Pyrol. 64, 421–431.
Elzaki, O.T., Khider, T.O., 2013. Strength properties of Ailanthus excels Roxb (tree of heaven) from western Sudan. J. Appl. Indust. Sci. 1, 38–40.
Fengel, D., Wegener, G., 1989. Wood: Chemistry, Ultrastructure, Reactions, second ed. Walter de Gruyter, Berlin, Germany, p. 613.
Iiyama, K., Pant, R., 1988. The mechanism of the Maule colour reaction. Introduction of methylated syringyl nuclei in softwood lignin. Wood Sci. Technol. 22, 167–175.
Johansen, D.A., 1940. Plant Microtechnique. McGraw Hill, New York.

Kleist, G., Schmitt, U., 2001. Characterization of a softrot like decay pattern by *Coniophora puteana* (Schm.) Karst in Sapelli wood. Holzforschung 55, 573–578.
Koyani, R.D., Rajput, K.S., 2014. Light microscopic analysis of *Tectona grandis* L.f. wood inoculated with *Irpex lacteus* and *Phanerochaete chrysosporium*. Eur. J. Wood Wood Prod. 72, 157–164.
Koyani, R.D., Sanghvi, G.V., Bhatt, I.M., Rajput, K.S., 2010. Pattern of delignification in *Ailanthus excels* Roxb., wood by *Inonotus hispidus*. Mycology 1, 204–211.
Levin, L., Castro, M.A., 1998. Anatomical study of the decay caused by the white-rot fungus *Trametes trogii* (Aphyllophorales) in wood of *Salix* and *Populus*. Int. Assoc. Wood Anatom. J. 19, 169–180.
Luján, L.M.L., Murace, M.A., Keil, G.D., Otaño, M.E., 2004. Patterns of decay caused by *Pycnoporus sanguineus* and *Ganoderma lucidum* (Aphyllophorales) in poplar wood. Int. Assoc. Wood Anatom. J. 25, 425–433.
Micco, V.D., Aronne, G., 2007. Anatomical features, monomer lignin composition and accumulation of phenolics in 1 year old branches of the Mediterranean *Cistus ladanifer* L. Bot. J. Linn. Soc. 155, 361–371.
Robles, C.A., Carmaran, C.C., Lopez, S.L., 2011. Screening of xylaphagous fungi associated with *Platanus acerifoila* in urban landscapes: biodiversity and potential Biodeterioration. Landsc. Urban Plan. 100, 129–135.
Robles, C.A., Castro, M.A., Lopez, S.E., 2014. Wood decay by *Inonotus ricki* and *Bjerkandera adusta*: a micro and ultrastructural approach. Int. Assoc. Wood Anatom. J. 35, 51–60.
Sanghvi, G.V., Koyani, R.D., Rajput, K.S., 2013. Anatomical characterization of Teak wood (Tectona grandisL.f.) decayed by fungus *Chrysosporium asperatum*. J. Trop. For. Sci. 25, 547–553.
Schmitt, U., Luerer, B., Dujiesiefken, D., Koch, G., 2014. The Massaria disease of plane trees: its wood decay mechanism. Int. Assoc. Wood Anatom. J. 35, 395–408.
Schwarze, F.W.M.R., 2007. Wood decay under microscope. Fungal Biol. Rev. 21, 133–170.
Schwarze, F.W.M.R., Fink, S., 1997. Reaction zone penetration and prolonged persistence of xylem rays in London plane wood degradation by the basidiomycete *Inonatus hispidus*. Mycol. Res. 101, 1207–1214.
Schwarze, F.W.M.R., Lonsdale, D., Fink, S., 1995. Soft rot and multiple T-branching by the basidomycete *Inonotus hispidus* in ash and London plane. Mycol. Res. 99, 813–820.
Tamura, K., Nei, M., 1993. Estimation of the number of nucleotide substitutions in the control region of mitochondrial DNA in humans and chimpanzees. Mol. Biol. Evol. 10, 512–526.
Ward, G., Hadar, Y., Dosoretz, C.G., 2004. The biodegradation of lignocelluloses by white rot fungi. In: Arora, D.K. (Ed.), Fungal Biotechnology in Agricultural Food, and Environmental Applications. Marcel Dekker, New York, pp. 393–407.
Worall, J.J., Anagnost, S.E., Zabel, R.A., 1997. Comparison of wood decay among diverse lignicolus fungi. Mycologia 89, 199–219.